the curie (Ci), which is equal to 3.7×10^{10} Bq.* In geochemistry, however, activity is often simply expressed in units of *disintegrations per minute* (dpm) per gram or per mole (1 dpm = 60 Bq/g) and is denoted by writing parentheses around the isotope (or the isotope ratio). Thus (^{234}U) is the activity of ^{234}U.

The state of *radioactive equilibrium* is the condition where the *activities* of the daughter and the parent are equal:

$$\boxed{\frac{dN_D}{dt} = \frac{dN_P}{dt}} \qquad (8.39)$$

where the derivatives refer to the activities of parent and daughter. It shares the same fundamental characteristic as the chemical equilibrium state: it is the state that will eventually be achieved if the system is not perturbed (remains closed). We can demonstrate this is so in two ways. The first is a simple mathematical demonstration. The equilibrium state is the steady state where the abundance of the daughter does not change, and so the left-hand side of eqn. 8.36 is zero:

$$0 = \lambda_P N_P - \lambda_D N_D \qquad (8.40)$$

We substitute the dN/dt terms for the λN terms in eqn. 8.40, rearrange, and we obtain eqn. 8.39 as predicted.

The second demonstration is a thought experiment. Imagine a hopper, a grain hopper with an open top and a door in the bottom. The door is spring-loaded such that the more weight is placed on the door, the wider it opens. Suppose we start dropping marbles into the hopper at a constant rate. The weight of marbles accumulating in the hopper will force the door open slightly and marbles will start falling out at a slow rate. Because the marbles are falling out more slowly than they are falling in, the number and weight of marbles in the hopper will continue to increase. As a result, the door will continue to open. At some point, the door will be open so wide that marbles are falling out as fast as they are falling in. This is the steady state. Marbles can no longer accumulate in the hopper and hence the door is not forced to open any wider. The marbles falling into the door are like the decay of the parent isotope. The marbles in the hopper represent the population of daughter isotopes. Their decay is represented by their passing through the bottom door. Just as the number of marbles passing through the door depends on the number of marbles in the hopper, the activity (number of decays per unit time) of an isotope depends on the number of atoms present.

If the rate of marbles dropping into the hopper decreases for some reason, marbles will fall out of the hopper faster than they fall in. The number of marbles in the hopper will decrease; as a result the weight on the door decreases and it starts to close. It continues to close (as the number of marbles decreases) until the rate at which marbles fall out equals the rate at which marbles fall in. At that point, there is no longer a change in the number of marbles in the hopper and the position of the door stabilizes. Again equilibrium has been achieved, this time with fewer marbles in the hopper, but nevertheless at the point where the rate of marbles going in equals the rate of marbles going out. The analogy to radioactive decay is exact.

Thus when a system is disturbed it will ultimately return to equilibrium. The rate at which it returns to equilibrium is determined by the decay constants of the parent and daughter. If we know how far out of equilibrium the system was when it was disturbed, we can determine the amount of time that has passed since it was disturbed by measuring the present rate of decay of the parent

* The Becquerel is named in honor of physicist Henri Becquerel (1952–1908) who serendipitously discovered radioactivity in 1896 when he left some uranium ore on photograph plates and found the plates exposed. The Curie is named in honor of Marie Curie (1867–1934), who was Becquerel's doctoral student and whose pioneering work in radioactivity won her the 1903 Nobel Prize in physics jointly with her husband Pierre Curie and Henri Becquerel. In 1911 she won the Nobel Prize in chemistry for having discovered the elements radium and polonium (the latter named for her native Poland). Marie Curie remains the first and only person to have won Nobel prizes in two fields of science. She died in 1934 from radiation poisoning, a year before her daughter Irène Joliot-Curie won the Nobel Prize for chemistry jointly with her husband.

and daughter. Equilibrium is approached asymptotically, and these dating schemes are generally limited to time-scales of less than 5–10 times the half-life of the daughter. At longer times, the difference between actual activities and equilibrium becomes too small to measure reliably.

There are several useful dating methods based on the degree of disequilibria between U decay series nuclides. Our first example is ^{234}U–^{238}U dating of sediments. As may be seen from Figure 8.19, ^{234}U, which has a half-life of 246,000 years, is the "great-granddaughter" of ^{238}U. For most purposes, the half-lives of the two intermediate daughters ^{234}Th and ^{234}Pa are so short that they can be ignored (because they quickly come into equilibrium with ^{238}U). As it turns out, ^{234}U and ^{238}U in seawater are not in equilibrium – the $^{234}U/^{238}U$ activity ratio is not 1. It is fairly constant, however, at about 1.15. The reason for this disequilibrium is that ^{234}U is preferentially leached from rocks because ^{234}U is present in minerals in damaged sites. It occupies the site of a ^{238}U atom that has undergone α-decay. The α particle and the recoil of the nucleus damage this site. Since it occupies a damaged site, it is more easily leached or dissolved from the crystal during weathering than ^{238}U. The oceans collect this "leachate", hence they are enriched in ^{234}U. When U enters a sediment it is isolated from seawater (not necessarily immediately) and ^{234}U decays faster than it is created by decay of ^{238}U, so it slowly returns to the equilibrium condition where $(^{234}U/^{238}U) = 1$.

Let's now consider the problem from a mathematical perspective and derive an equation describing this return to equilibrium. We can divide the ^{234}U activity in a sample into that which is *supported* by ^{238}U (i.e., that amount in radioactive equilibrium with ^{238}U), and that amount that is excess (i.e., *unsupported* by ^{238}U):

$$(^{234}U) = (^{234}U)_s + (^{234}U)_u \qquad (8.41)$$

Subscripts *s* and *u* denote supported and unsupported. The activity of the excess ^{234}U decreases with time according to eqn. 8.4, which we can rewrite as:

$$(^{234}U)_U = (^{234}U)^0_U e^{-\lambda_{234} t} \qquad (8.42)$$

where the superscript nought denotes the initial unsupported activity (at $t = 0$). We can also write:

$$(^{234}U)^0_U = (^{234}U)^0 - (^{234}U)_s \qquad (8.43)$$

which just says that the initial unsupported activity of ^{234}U is equal to the total initial activity of ^{234}U minus the (initial) supported activity of ^{234}U. *Since to a very good approximation the activity of the parent, ^{238}U, does not change over time on the order of the half-life of ^{234}U or even ten half-lives of ^{234}U, the present ^{238}U activity is equal to the activity at $t = 0$* (we make the usual assumption that the system is closed). By definition the supported activity of ^{234}U is equal to the activity of ^{238}U, both now and at t = 0, hence eqn. 8.41 can be expressed as:

$$(^{234}U) = (^{238}U) + (^{234}U)_u \qquad (8.44)$$

and eqn. 8.43 becomes

$$(^{234}U)^0_u = (^{238}U) + (^{234}U)_u \qquad (8.45)$$

Substituting eqn. 8.45 into 8.42 yields:

$$(^{234}U)_u = \left[(^{234}U)^0 - (^{238}U)\right] e^{-\lambda_{234} t} \qquad (8.46)$$

Substituting eqn. 8.46 into 8.44, we have:

$$(^{234}U) = (^{238}U) + \left[(^{234}U)^0 - (^{238}U)\right] e^{-\lambda_{234} t} \qquad (8.47)$$

Just as for other isotope systems, it is generally most convenient to deal with ratios rather than absolute activities (among other things, this allows us to ignore detector efficiency, provided the detector is equally efficient at all energies of interest), hence we divide by the activity of ^{238}U:

$$\left(\frac{^{234}U}{^{238}U}\right) = 1 + \left[\frac{(^{234}U)^0 - (^{238}U)}{(^{238}U)}\right] e^{-\lambda_{234} t} \qquad (8.48)$$

or since $^{238}U = {}^{238}U^0$:

$$\left(\frac{^{234}U}{^{238}U}\right) = 1 + \left[\left(\frac{^{234}U}{^{238}U}\right)^0 - 1\right] e^{-\lambda_{234} t} \qquad (8.49)$$

Corals, for example, concentrate U. If we measure the $(^{234}U/^{238}U)$ ratio of an ancient coral, and can assume that the seawater in which that coral grew had a $(^{234}U/^{238}U)$ the

same as modern seawater (1.15), then the age of the coral can be obtained by solving eqn. 8.49 for t.

Because the disequilibrium between ^{230}Th and ^{238}U can be much larger than between ^{234}U and ^{238}U, ^{230}Th–^{238}U disequilibria is a more commonly used dating scheme than is ^{234}U–^{238}U. ^{230}Th is the daughter of ^{234}U (the decay chain is $^{238}\text{U} \rightarrow {}^{234}\text{Th} + \alpha$, $^{234}\text{Th} \rightarrow {}^{234}\text{Pa} + \beta^-$, $^{234}\text{Pa} \rightarrow {}^{234}\text{U} + \beta^-$, $^{234}\text{U} \rightarrow {}^{230}\text{Th} + \alpha$). To simplify the math involved, let's assume ^{234}U and ^{238}U are in radioactive equilibrium. In high-temperature systems, this is a very good assumption because α–damaged sites, which cause the disequilibrium noted earlier, are quickly annealed. With this assumption, we can treat the production of ^{230}Th as if it were the direct decay product of ^{238}U. We write an equation analogous to 8.41 and from it derive an equation analogous to 8.47:

$$(^{230}\text{Th}) = (^{238}\text{U}) + \left[(^{230}\text{Th})^0 - (^{230}\text{U})\right] e^{-\lambda_{230} t} \tag{8.50}$$

We divide by the activity of ^{232}Th:

$$\left(\frac{^{230}\text{Th}}{^{232}\text{Th}}\right) = \left(\frac{^{238}\text{U}}{^{232}\text{Th}}\right) + \left[\left(\frac{^{230}\text{Th}}{^{232}\text{Th}}\right)^0 - \left(\frac{^{238}\text{U}}{^{232}\text{Th}}\right)\right] e^{-\lambda_{230} t} \tag{8.51}$$

and rearranging:

$$\left(\frac{^{230}\text{Th}}{^{232}\text{Th}}\right) = \left(\frac{^{230}\text{U}}{^{232}\text{Th}}\right)^0 e^{-\lambda_{230} t} + \left(\frac{^{238}\text{U}}{^{232}\text{Th}}\right)(1 - e^{-\lambda_{230} t}) \tag{8.52}*$$

^{230}Th/^{238}U is commonly used to date sediments and to determine sedimentation rates. However, unlike the case of $(^{234}\text{U}/^{238}\text{U})^0$, $(^{230}\text{Th}/^{232}\text{Th})^0$ is not known *a priori*, so there are two unknowns in eqn. 8.52. As was the case for isochrons, however, we can solve for these two unknowns if we have a series of two or more measurements on sediments with the same initial $(^{230}\text{Th}/^{232}\text{Th})$. Example 8.5 demonstrates how this is done for the case of a Mn nodule. In other cases, corals, for example, we can assume that $(^{230}\text{Th}/^{232}\text{Th})^0$ is the same as in modern seawater.

Th–U disequilibria may also be used for dating lavas, and we now turn our attention briefly to this application. Equation 8.52 has the form of a straight line on a $(^{230}\text{Th}/^{232}\text{Th})$–$(^{238}\text{U}/^{232}\text{Th})$ plot; the first term is the intercept and $(1 - e^{-\lambda_{230} t})$ is the slope. Since the slope is proportional to time, a line on a $(^{230}\text{Th}/^{232}\text{Th})$–$(^{238}\text{U}/^{232}\text{Th})$ plot is an isochron, though unlike a conventional isochron the intercept also changes with time (Figure 8.21).

To understand how this works, imagine a crystallizing magma with homogenous $(^{230}\text{Th}/^{232}\text{Th})$ and $(^{238}\text{U}/^{232}\text{Th})$ ratios. Th and

Example 8.5 Determining the growth rate of a Mn nodule

The tops of manganese nodules grow by precipitation of Mn–Fe oxides and hydroxides from seawater. They are known to grow very slowly, but how slowly? If we assume the rate of growth is constant, then depth in the nodule should be proportional to time. If z is the depth in the nodule, and s is the growth (sedimentation) rate, then:

$$t = z/s \tag{8.53}$$

and eqn. 8.52 becomes:

$$\left(\frac{^{230}\text{Th}}{^{232}\text{Th}}\right) = \left(\frac{^{230}\text{Th}}{^{232}\text{Th}}\right)^0 e^{-\lambda_{230} z/s} + \left(\frac{^{238}\text{U}}{^{232}\text{Th}}\right)(1 - e^{-\lambda_{230} z/s}) \tag{8.54}$$

(*Continued*)

* This equation may also be derived directly from eqn. 8.37 since $\lambda_{230} - \lambda_{238} \cong \lambda_{230}$, $^{238}\text{U} \cong {}^{238}\text{U}^\circ$, and $e^{-\lambda_{238} t} \cong 1 \cong 1$ for any value of t over which this method is useful (~500,000 years).

At the surface of the nodule, $z = 0$, so the exponential terms both go to 1 and the measured activity ratio is the initial activity ratio. Having a value for $(^{230}Th/^{232}Th)^0$, eqn. 8.54 can then be solved for s, the growth rate, if measurements are made at some other depth.

In practice, however, it is difficult to obtain a sample exactly at the surface: a finite amount of material is required for analysis, and this often translates into a layer of several mm thickness. Equation 8.54 is solved in that instance by less direct means. For example, consider the data shown in Figure 8.20 on a Pacific manganese nodule reported by Huh and Ku (1984). In this plot of $(^{230}Th/^{232}Th)$ vs. depth, the initial ratio is the intercept of the best-fit line through the data. A growth rate was obtained by making an initial guess of the initial $(^{230}Th/^{232}Th)$ ratio, then iteratively refining the solution to eqn. 8.54 by minimizing the difference between computed and observed activity ratios. A growth rate of 49.5 mm/Ma and $(^{230}Th/^{232}Th)$ of 77.7 was found to best fit the observations.

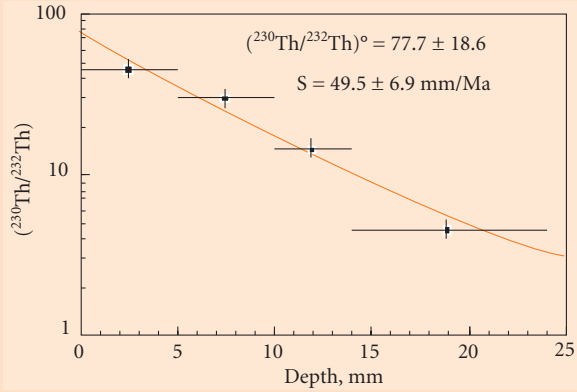

Figure 8.20 $(^{230}Th/^{232}Th)$ as a function of depth in a manganese nodule from MANOP Site H. After Huh and Ku (1984). With permission from Elsevier.

U partition into different minerals differently, so the minerals will have variable $(^{238}U/^{232}Th)$ ratios but constant $(^{230}Th/^{232}Th)$ ratios (assuming crystallization occurs quickly compared with the half-life of Th) since these two isotopes are chemically identical. Thus the minerals will plot on a horizontal line in Figure 8.21 at $t = 0$. After the system closes, ^{238}U and ^{230}Th will begin to come to radioactive equilibrium (either ^{230}Th will decay faster than it is produced or vice versa, depending on whether $(^{230}Th/^{238}U)$ is greater than or less than 1, the equilibrium value). Thus the original horizontal line will rotate, as in a conventional isochron diagram, but unlike the conventional isochron diagram, the intercept also changes. The rotation occurs about the point where $(^{230}Th/^{232}Th) = (^{238}U/^{232}Th)$, which is known as the *equipoint*. As t approaches infinity, the exponential term approaches 1 and:

$$\lim_{t\to\infty}\left(\frac{^{230}Th}{^{232}Th}\right) = \left(\frac{^{238}Th}{^{232}Th}\right) \qquad (8.55)$$

Thus the equilibrium situation, at $t = \infty$, is $(^{230}Th/^{232}Th) = (^{238}U/^{232}Th)$. In this case, all the minerals will fall on a line, having a slope of 1. This line is known as the *equiline*.

^{226}Ra is another relatively long-lived nuclide ($t_{1/2} = 1600$ yr) that has proved useful in dating igneous rocks. The fundamentals are precisely analogous to those we have discussed for ^{234}U and ^{230}Th, with one exception. Unfortunately, Ra has no stable isotope to which one can ratio ^{226}Ra. Therefore, the assumption is made that Ra behaves as Ba, and the abundance of Ba is used to form a ratio.

Figure 8.22a shows a ^{230}Th–^{238}U mineral isochron obtained on a peralkaline lava from the African Rift Valley in Kenya (Black *et al.*,

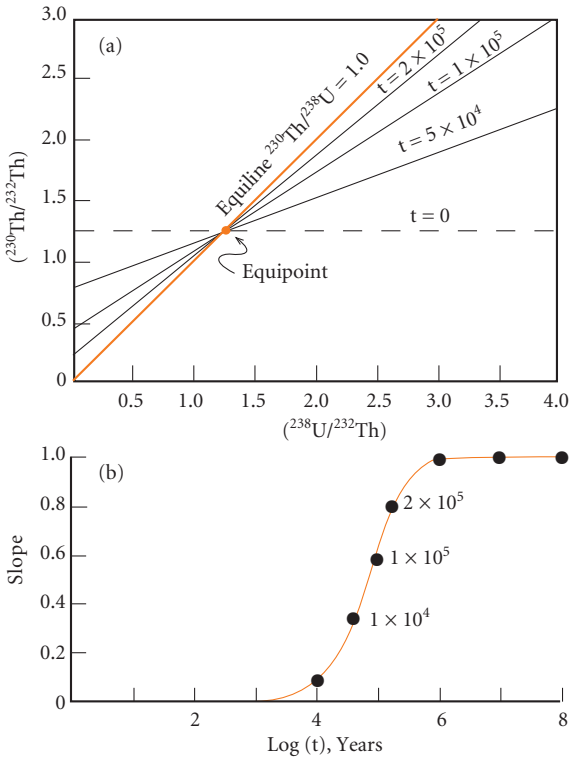

Figure 8.21 (a) ^{230}Th–^{238}U isochron diagram. The $(^{238}U/^{232}Th)$ of the source is given by the intersection of the isochron with the equiline. (b) This shows how the slope changes as a function of time. After Faure (1986). With permission from John Wiley & Sons.

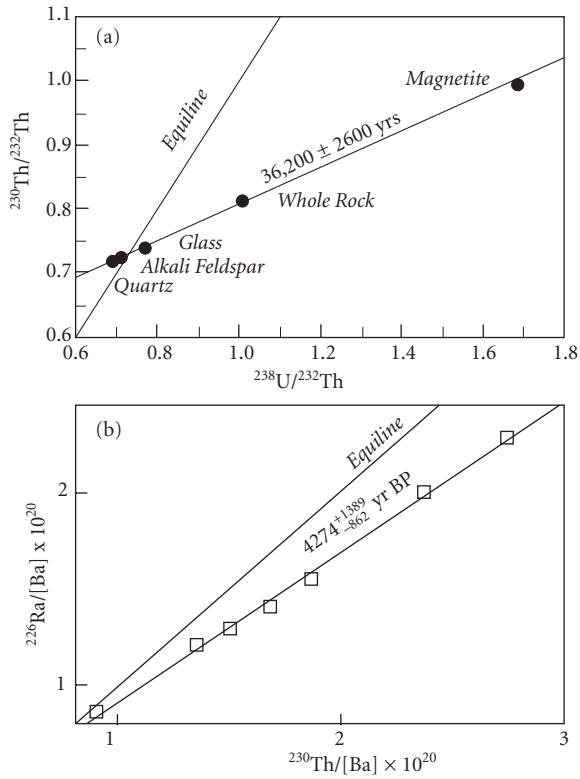

Figure 8.22 (a) ^{230}Th–^{238}U mineral isochron on a commendite lava from Kenya. After Hawkesworth *et al.* (2000). With permission from Oxford University Press. (b) ^{226}Ra–^{230}Th whole rock isochron on trachyte lavas from Longonot volcano in Kenya. After Black *et al.* (1997). With permission from Oxford University Press.

1997) which yields an age of 36,200 ± 2600 yrs. However, the eruption age of this lava is constrained by stratigraphy and ^{14}C dating to be less than 9000 yrs. Other lavas in the area yielded similarly precise, but anomalously old, U–Th ages. Black *et al.* interpreted the ages to reflect the time of crystallization of the phenocrysts, which in this case pre-dates eruption by >25,000 yrs. Figure 8.22b shows a ^{226}Ra–^{230}Th whole-rock isochron from trachytes of Longonot volcano, also in the African Rift Valley in Kenya (Hawkesworth *et al.*, 2000). The isochron age, 4724 yrs, is consistent with other geochronological techniques that constrain the age to be 5650–3280 yrs.

In the past, the activities of U-decay series isotopes were measured by alpha-counting and fairly large quantities of material were necessary. Improvements in mass spectrometry made it possible to measure ^{234}U, ^{230}Th, and other key nuclides such as ^{231}Pa and ^{226}Ra with smaller quantities of material and much better precision than α-counting. This has led to a considerable expansion of applications of U-decay series isotopes.

8.4.8 Isotopes of He and other rare gases

8.4.8.1 Helium

Alpha particles are, of course, simply ^4He nuclei, and therefore ^4He is produced by alpha decay of U and Th. Thus the ratio of $^4He/^3He$ varies in the Earth. Unlike virtually all other elements, He is not conserved on the Earth: much of the He present when the Earth formed has been subsequently lost. Being a rare gas, He does not combine chemically with anything, and it also diffuses rapidly (ever had a helium balloon? How long did it last?) Helium brought to the Earth's surface by magmatism eventually finds its way into

the atmosphere. Once there, it can escape from the top of atmosphere because of its low mass.* (H^2 also escapes from the atmosphere, but most H is bound up as water or hydrous minerals, so relatively little is lost.) Since ^{4}He is continually produced and, for all practical purposes, ^{3}He is not, it should not be surprising that the ^{4}He/^{3}He ratio in the Earth is a very large number. For some reason, perhaps because geochemists like to deal with very small numbers rather than very large ones, or perhaps because it is actually ^{3}He that is most interesting, the He isotope ratio is generally expressed as ^{3}He/^{4}He, in contradiction to the normal convention of placing the radiogenic isotope in the numerator. We will adhere to this particular convention of not adhering to the convention and use the ^{3}He/^{4}He ratio.

The ^{3}He/^{4}He ratio of the atmosphere is 1.384×10^{-6}. Since this ratio is uniform and atmospheric He is available to all laboratories, it is a convenient standard and moreover provides the basis for a convenient normalization. He isotope ratios are often reported and discussed relative to the atmospheric value. The units are called simply R/R_A, where R_A indicates the atmospheric ratio.

Actually, it is not quite true that ^{3}He is not produced in the Earth. It is produced in very small quantities through the nuclear reaction: $^6\text{Li}(n,\alpha)\rightarrow{}^3\text{H}(\beta)\rightarrow{}^3\text{He}$, which is to say ^{6}Li is excited by the capture of a neutron that has been produced by U fission, and decays through the emission of an alpha particle to tritium, which beta-decays to ^{3}He. As a result He in crustal rocks has an $R/R_A \approx 0.1$–0.01 (the exact ratio varies with the Li/U ratio). ^{3}He can also be produced in the atmosphere and surface of the Earth by cosmic ray spallation reactions. Up to about 35 years ago, all He was thought to be a product of these processes (radiogenic and cosmogenic). Then helium with R/R_A around 1.22 was discovered in Pacific deep water in 1969 (Clark *et al.*, 1969). Subsequently, Lupton and Craig (1975) discovered that mid-ocean ridge basalt glasses had high ^{3}He/^{4}He ratios. The gases are trapped in the glassy rims of basalts by the combined effects of hydrostatic pressure and rapid quenching. Measurements in 1974 and 1975 found such basalts had $R/R_A \approx 9$. It was clear that a "primordial" He component was trapped in the Earth's interior and is constantly escaping. Subsequent measurements have shown that the ^{3}He/^{4}He of MORB is quite uniform around $R/R_A \approx 8.5 \pm 1$. This is only primordial in a relative sense: gas-rich meteorites have an $R/R_A \approx 200$. Thus even in MORB, He is 95% radiogenic.

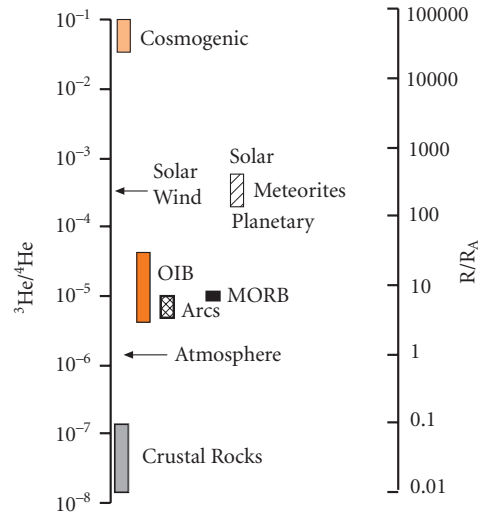

Figure 8.23 He isotope ratios in various terrestrial and solar system materials. "Solar" and "Planetary" refer to the solar and planetary components in meteorites. "Crustal rocks" shows the values expected for *in situ* production from α-decay and neutron-induced nuclear reactions.

Figure 8.23 illustrates the He isotopic composition of various terrestrial reservoirs. Oceanic islands and other hotspots often have even higher ratios, up to about $R/R_A \approx 40$, though some islands, Tristan da Cunha for example, have lower ratios: $R/R_A \approx 5$ (e.g., Kurz *et al.*, 1982). This suggests that most oceanic island basalts are derived from a less degassed, and in that sense more primordial, reservoir than MORB. This is consistent with the mantle plume hypothesis.

* At equilibrium the average kinetic energy of all varieties of molecules in a gas will be equal. Since kinetic energy is related to velocity by $E = \frac{1}{2}mv^2$, and since the mass of He is lower than for other species, the velocities of He atoms will be higher and more likely to exceed the escape velocity. In actuality, however, escape of He is more complex than simple thermal acceleration and involves other processes such as acceleration of He ions by the Earth's magnetic field.

Island arc volcanics (IAV) also seem to be fairly uniform, with $R/R_A \approx 6$ (Lupton, 1983). Ratios lower than MORB suggest the presence of a slab-derived component, but also indicate most of the He in IAV comes from the mantle wedge (a conclusion similar to the one reached from other radiogenic isotopes).

Two interesting developments are the discovery of cosmogenic He in Hawaiian basalts (Kurz, 1987), and very high R/R_A in some very slowly accumulating marine sediments. The former is a result of the $^6Li(n,\alpha)\rightarrow{}^3H(\beta)\rightarrow{}^3He$ reaction instigated by cosmic-ray produced neutrons and spallation.* The cosmogenic component decreases rapidly with depth of the rock (it is largely restricted to the top meter) and increases with elevation above sea-level (the effect was noticed at the summit of Haleakala at 2000 m). Thus one should be suspicious of high $^3He/^4He$ ratios in old (100,000 yrs or more) sub-aerial rocks. R/R_A as high as 226 (and as low as 0.03) have also been observed in diamonds. The meaning of this was not immediately clear, but the origin of these diamonds is unknown, and the most probable explanation is that the diamonds were mined from a placer and that the He is cosmogenic. Very high R/R_A in some very slowly accumulating marine sediments is probably an effect of accumulation of cosmic dust in sediment. $^{40}Ar/^{36}Ar$ ratios lower than atmospheric have also been observed in deep-sea sediment, which is also suggestive of a cosmic origin. A final development was the realization that He ratios of magma could change, through the combined effects of diffusion out of the magma and radiogenic growth of He, on the time-scale of the residence time of magma in a magma chamber (Zindler and Hart, 1986). This means we must be cautious of low $^3He/^4He$ ratios as well.

Since He is injected at mid-ocean ridges, particularly in the Pacific, at depths of 2500–3000 meters, He isotopes can be used to trace water mass movements. Figure 8.24 shows the He plume of hydrothermal activity on the East Pacific Rise. Interestingly, the plume indicates water is flowing in the direction opposite to that which the physical oceanographers had thought. Another application is prospecting for ridge-crest hydrothermal activity. Several hydrothermal areas (including the first one) have been discovered from He isotope anomalies in the water column. ^4He is also used as a tracer in U prospecting.

8.4.8.2 Neon

Neon has perhaps the most puzzling isotopic systematics of the noble gases. Ne has three isotopes, ^{20}Ne, ^{21}Ne, and ^{22}Ne. Though none of them are radiogenic, the isotopic composition of neon varies in the Earth as well as extraterrestrial materials (Figure 8.25). Two processes have apparently produced these

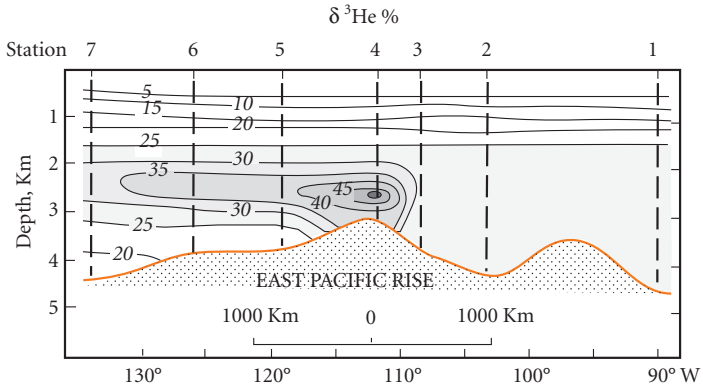

Figure 8.24 Contours of relative ^3He concentrations in seawater over the East Pacific Rise (Lupton and Craig, 1975). With permission from Elsevier.

* Spallation is the process by which a nucleus breaks into smaller nuclei as a result of a collision with a very high-energy particle such as a cosmic ray.

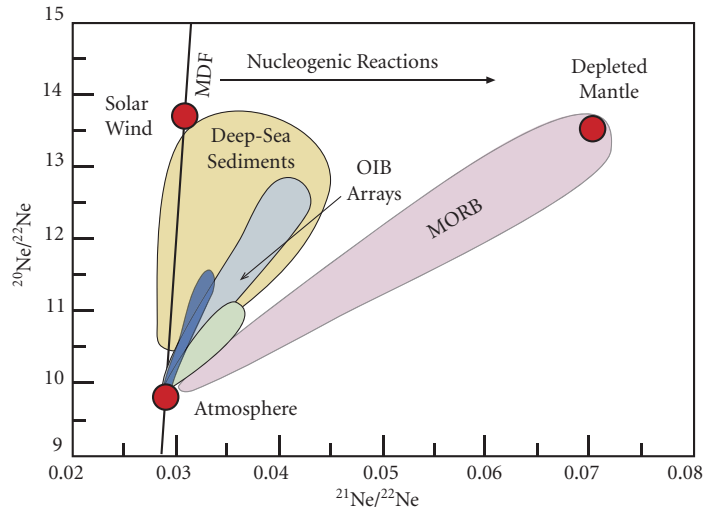

Figure 8.25 Ne isotope ratios in terrestrial materials. The line marked "MDF" is the mass dependent fractionation line. The line has a slope of 2 because the change in $^{20}Ne/^{22}Ne$ resulting from fractionation should be twice that of $^{21}Ne/^{22}Ne$ because the mass difference between ^{20}Ne and ^{22}Ne is twice that between ^{21}Ne and ^{22}Ne. OIB arrays are data fields for basalts and mantle xenoliths from Samoa and Hawaii.

isotopic variations: mass-dependent fractionation (which we cover in the next chapter) and nuclear reactions such as $^{18}O(\alpha,n)\rightarrow {}^{21}Ne$, $^{24}Mg(n,\alpha)\rightarrow {}^{21}Ne$, and $^{25}Mg(n,\alpha)\rightarrow {}^{22}Ne$, with the α particles and neutrons coming from α-decay and fission respectively. Production rates are quite small, for example about 4.2×10^{-s22} cc/g of ^{21}Ne in the mantle. The production rate of ^{21}Ne is about an order of magnitude higher than that of ^{20}Ne and ^{22}Ne, and ^{21}Ne is the least abundant of the Ne isotopes (0.27%), so the effect of these reactions is to increase the $^{21}Ne/^{22}Ne$ ratio without changing the $^{20}Ne/^{22}Ne$ ratio. In addition, nucleosynthetic processes are apparently responsible for some of the Ne isotopic variations in meteorites (see Chapter 10).

Noble gases trapped in basalts from mid-ocean ridges and basalts and mantle xenoliths from oceanic islands form arrays that diverge from atmospheric composition to compositions with higher $^{20}Ne/^{22}Ne$ and $^{21}Ne/^{22}Ne$ (e.g., Sarda *et al.*, 1988; Poreda and Farley, 1992). According to Farley and Poreda (1993), the array reflects contamination of mantle Ne by atmospheric Ne; in essence, they are mixing arrays between mantle components with high $^{20}Ne/^{22}Ne$ and variable $^{21}Ne/^{22}Ne$ ratios. The very low concentrations of He in the atmosphere minimizes the problem of contamination in basalts; but atmospheric concentrations of the heavier noble gases, including Ne, are higher, so this is much more of a problem in the case of these gases.

Even though the arrays themselves are the products of contamination, the variation in the slope of the arrays is significant and indicates variation of $^{21}Ne/^{22}Ne$ in the mantle, with the MORB source having higher $^{21}Ne/^{22}Ne$ and OIB sources. This would be consistent with the MORB source being more degassed and hence having lower Ne concentrations. Addition of nucleogenic Ne would have a larger effect on $^{21}Ne/^{22}Ne$ in that case.

Two hypotheses have been proposed to explain the observed isotopic variations in the Earth. In the model advocated by Japanese workers (e.g., Honda *et al.*, 1991; Ozima and Zahnle, 1993), the Earth initially formed with a Ne isotopic composition similar to that of solar wind. During the Earth's very early history, much of Earth's atmophile element inventory escaped from the interior, perhaps during the existence of a magma ocean, to form a hot, massive atmosphere. Much of the hydrogen and helium and a significant fraction of the neon escaped the atmosphere

during this time. The efficiency of escape will depend on the mass of the molecule, so that the proportional loss of ^{20}Ne is greatest and that of ^{22}Ne the least. Thus the isotopic composition of the residual atmosphere has lower ^{20}Ne/^{22}Ne and ^{21}Ne/^{22}Ne than the original one.

Subsequently, the ^{21}Ne/^{22}Ne in the degassed mantle increased due to nucleogenic production of ^{21}Ne. Portions of the mantle that experienced greater degassing should have higher ^{21}Ne/^{22}Ne than less degassed portions. Thus MORB apparently samples the most degassed mantle, presumably the upper mantle, while oceanic island basalts and xenoliths are apparently derived from a less degassed part of the mantle, presumably mantle plumes originating in the deep mantle.

Allègre *et al*. (1993) proposed a somewhat different model, one inspired by the observation that slowly accumulating pelagic sediments have Ne isotope ratios different from atmospheric ratios, apparently due to the presence of cosmic dust and micrometeorites in the sediment. They suggest that the Earth originally formed with a Ne isotopic composition similar to the present mantle. Subduction of deep sea sediments then increased the ^{20}Ne/^{22}Ne ratio of the degassed mantle. Nucleogenic production in the mantle then increased the ^{21}Ne/^{22}Ne ratio, and this effect has been greatest in the most degassed portion of the mantle, which is presumably sampled by MORB.

8.4.8.3 K–Ar–Ca

There are several aspects of the K–Ar system that make it particularly advantageous for some geochronological applications. First, ^{40}K has one of the shortest half-lives of the decay systems in Table 8.2, making it more useful for dating young rocks than other systems. In favorable cases, K–Ar ages on rocks as young as 30,000 yrs can be obtained with useful precision. Second, Ar is a rare gas and it is virtually totally lost upon eruption in most lavas. With no initial component, an age can be obtained from a single K–Ar determination. Being a rare gas, Ar diffuses somewhat more readily than other elements. Further, K is concentrated in sheet silicates such as micas, which have comparatively open crystal structures. As a result, the closure temperature for the K–Ar system is low, making it a useful system for study of relatively low-temperature phenomena (such as petroleum genesis). This, of course, can be a disadvantage, as it means the K–Ar system is reset rather easily.

From a geochemical viewpoint, the K–Ar system is of most interest with respect to the degassing of the Earth and evolution of the Earth's atmosphere. The most important questions in this regard are: what proportion of the Earth has been degassed, how extreme has this outgassing been, and when did this degassing occur? To briefly illustrate how K–Ar systematics can address these problems, consider the second question. We can think of two extreme possibilities: outgassing occurred yesterday; outgassing occurred simultaneously with the formation of the Earth. If outgassing occurred yesterday, then the ^{40}Ar/^{36}Ar ratio of the Earth's interior will be the same as that of the atmosphere. If outgassing occurred early in Earth's history, then the ^{40}Ar/^{36}Ar ratio of the atmosphere should be close to the initial ratio for the solar system and the ^{40}Ar/^{36}Ar of the Earth's interior should be much higher because of the decay of ^{40}K over the history of the Earth. In actuality, neither of these models matches observation. The ^{40}Ar/^{36}Ar ratio measured in MORB, in which noble gases are trapped by the pressure prevailing on the ocean floor, is very much higher than in the atmosphere. Ratios in MORB can be as high as 40,000, whereas that of the atmosphere is uniform at 295.5. So the Earth did not outgas yesterday. On the other hand, the atmospheric ratio is much higher than the solar system initial ^{40}Ar/^{36}Ar ratio. Indeed, the solar system initial ratio is less than 1, so most of the Ar in the atmosphere is actually radiogenic. Consequently, we can conclude that substantial degassing occurred after the Earth formed.

Now let's consider the first question: how much of the Earth has degassed? As we mentioned, essentially all the Ar in the atmosphere is radiogenic. Since both the concentration of Ar and its isotopic composition are uniform in the atmosphere, it is fairly easy to estimate the amount of ^{40}Ar in the atmosphere, which works out to be 1.65×10^{18} moles. The K concentration is the silicate part of the Earth is about 200 ± 50 ppm, which corresponds to $2.05 \pm 0.5 \times 10^{22}$ moles of K. Over the 4.5 Ga

of Earth's history, this amount of K should have produced about $2.8 \pm 0.7 \times 10^{18}$ moles of Ar. Thus about $60 \pm 15\%$ of the Ar that we expect has been produced by radioactive decay in the present atmosphere; the remainder must still be in the solid Earth. It is fairly easy to show that most of this must be in the mantle rather than the crust (Allegre *et al.*, 1996). The uncertainty associated with this estimate, which is due to the uncertainty about the K content of the Earth, is rather large however. At the one extreme, more than 50% of the Earth's ^{40}Ar remains in the mantle, suggesting a large volume of undegassed mantle; at the other extreme, 75% of the Earth ^{40}Ar has been released to the atmosphere.

Combining Ar systematics with isotope systematics of other noble gases, there seems to be consensus on these points: (1) the Earth probably lost its early, primitive atmosphere; (2) the present atmosphere is a product of degassing of the Earth's interior; (3) a substantial fraction of the mantle has been degassed, presumably through melting and volcanism; and (4) most of the degassing occurred early in Earth's history, probably shortly after it formed. Beyond these points, there is considerable disagreement.

Most of ^{40}K (90%) decays to ^{40}Ca. But this decay scheme has not yielded much geochemical or geochronological information thus far. The reason is the low ratio of ^{40}K to ^{40}Ca in most geological materials, which in turn means the radiogenic contribution to ^{40}Ca is small and ^{40}Ca/^{42}Ca variations are very small. Also, since the isotopes are rather light, they are comparatively easily fractionated. Indeed, it has been shown that they can be fractionated by the chemical techniques used to separate Ca. The variation of ^{40}Ca/^{42}Ca is so small that in one good geochronological age determination, the initial ^{40}Ca/^{42}Ca ratio of the Pike's Peak batholith (age 1 Ga) was found to be indistinguishable from the initial ratio in meteorites. Work by Marshall and DePaolo (1987) showed that MORB has ε_{Ca} values (ε_{Ca} is defined in exactly the same sense as ε_{Nd} and ε_{Hf}) of around 0. Thus although the source of mid-ocean ridge basalts has been depleted in K relative to Ca, this has not produced Ca isotope ratios significantly different from that of the bulk Earth. As a result of high K/Ca ratios, crustal rocks have slightly positive ε_{Ca} ratios. Interestingly, a number of island arc volcanics have ε_{Ca} in the range of 1–2, which is consistent with the hypothesis that their source contains a crustal component, a hypothesis based on their isotopic compositions of Pb, Sr and Nd.

8.5 COSMOGENIC AND FOSSIL ISOTOPES

The Earth is constantly bombarded by cosmic rays (we shouldn't feel picked on, the entire cosmos is). These are atomic nuclei (mostly H) stripped of their electrons and traveling at relativistic velocities. Some originate in the Sun, but most originate in high-energy regions of the cosmos such as supernovae. For the most part their origin is not well understood. What is understood is that they have sufficient energy to shatter a nucleus when they collide with one. The nucleus breaks into several parts in a process called *spallation*.

Having mass and charge, cosmic rays do not have much penetrating power. Thus the intensity of cosmic radiation increases with increasing altitude in the atmosphere (indeed, this is how they were shown to be of cosmic origin). Most are stopped in the atmosphere, their interactions creating a cascade of lower-energy particles, or are slowed considerably. Even if they do not score a direct hit, they lose energy through electromagnetic interaction with matter (ionizing the atoms they pass by). Thus cosmic rays have their greatest effect in the atmosphere and somewhat less of an effect in the uppermost few centimeters or so of rock.

The nuclear effects of cosmic radiation are on the whole pretty trivial. Nitrogen and oxygen, being the principal constituents of the atmosphere, are the most common targets, yet there is no change in the isotopic abundances of these elements. Cosmic radiation is most interesting because of the production of nuclides whose half-lives are so short they would not otherwise exist. The nuclides of greatest interest are listed in Table 8.5 along with their half-lives and their decay constants. These nuclides are created either directly through spallation (e.g., ^{10}Be), or by nuclear reactions with particles produced by spallation (e.g., ^{14}C: ^{14}N (n,p)$\rightarrow^{14}$C). We have space only to briefly consider a few of the many applications of cosmogenic nuclides.

Table 8.5 Some cosmogenic nuclides of geologic interest.

Nuclide	Half-life (yr)	λ (yr^{-1})
^{10}Be	1.5×10^6	0.462×10^{-6}
^{14}C	5730	0.1209×10^{-3}
^{26}Al	0.716×10^6	0.968×10^{-6}
^{36}Cl	0.308×10^6	2.25×10^{-6}
^{39}Ar	269	0.257×10^{-2}

8.5.1 ^{14}C

The best known of the cosmogenic nuclide dating methods is of course ^{14}C. It is useful in dating archeological, climatological, volcanological, seismological, and paleontological 'events'. Present technology utilizes accelerator mass spectrometry rather than traditional β-counting, and useful information on samples as old as 40,000 years can be produced. The principle of this method is quite simple. One assumes a constant production of ^{14}C in the atmosphere. The atmosphere is well mixed and has a uniform $^{14}C/^{12}C$ ratio. Carbon-14 isolated from the atmosphere by plants will decrease with time according to:

$$^{14}C = {}^{14}C^{\circ}e^{-\lambda t} \qquad (8.56)$$

If the production rate is constant, the "nought" value is the present-day atmospheric value. In practice, ^{14}C is generally reported in units of activity of ^{14}C per gram carbon – which is defined as the *specific activity*.

Research over the last 50 years has demonstrated that the production rate of ^{14}C has certainly not been constant, and it can be inferred from this that the cosmic ray flux has not been constant. The primary cause of this variation is variation in solar activity and the amount of solar wind. Solar wind consists of charged particles and the electromagnetic field associated it with deflects some fraction of cosmic rays that would otherwise enter the solar system and strike the Earth. In addition to this, the $^{14}C/^{12}C$ ratio in the present atmosphere is somewhat lower than it has been in the recent past, due to dilution with CO_2 released by extensive burning of fossil fuels.

To get around the problem of the non-constant production rate, ^{14}C ages have been calibrated by comparison with absolute ages derived from tree rings. This calibration has now been extended back about 12,000 years. Thus, accurate ^{14}C ages can be obtained despite production rate variations. Currently, an effort is under way to calibrate ^{14}C ages back 50,000 years by comparing them with $^{230}Th/^{238}U$ ages of corals. The discrepancy between ^{14}C ages and other chronometers such as tree rings and $^{230}Th/^{238}U$ ages provides a measure of the ^{14}C production rate and cosmic ray flux. That provides an indirect measure of past solar activity. Solar activity in turn has a direct effect on terrestrial climate, and hence must be constrained if past climatic variations are to be understood.

Other interesting applications include determining the "age" of deep water in the oceans. By comparing $^{14}C/^{12}C$ ratios of benthic and planktonic foraminifera in a single sedimentary horizon, it is possible to determine bottom-water ages in the past, and hence constrain "paleocirculation" rates.

Other cosmogenic isotopes have been used to determine sedimentation rates, growth rate of Mn nodules where ages are too old for U-series disequilibrium techniques, and the ages of ice in Greenland and Antarctic ice cores.

8.5.2 ^{36}Cl in hydrology

^{36}Cl has been applied to hydrological problems for some time. The general principle is that ^{36}Cl is produced at a constant rate in the atmosphere, carried to the surface of the Earth in rain and incorporated into hydrological systems. Cl is an excellent candidate element for such studies because it should remain in solution in most instances, and hence the only loss should be through radioactive decay. Imagine a simple system in which rainwater is incorporated into an aquifer at some unknown time in the past. In this case, if we can specify the number of ^{36}Cl atoms per liter in rain (and if we can assume this value is time-invariant), then we can determine the age of water in the aquifer by measuring the number of ^{36}Cl atoms per liter since:

$$^{36}Cl = {}^{36}Cl^{0}e^{-\lambda t} \qquad (8.57)$$

Determining the age of water in underground aquifers is an important problem because of the increasing demands placed in many parts

of the world on limited water resources. A prudent policy for water resource management is to withdraw from a reservoir at a rate no greater than the recharge rate. Determination of recharge rate is thus prerequisite to wise management.

Dealing with just the number, or concentration, of ^{36}Cl atoms can have disadvantages, and can be misleading. Evaporation, for example, would increase the number of ^{36}Cl atoms. Thus the ^{36}Cl/Cl ratio (Cl has two stable isotopes: ^{35}Cl and ^{37}Cl) is often used. This also can have problems since chlorine can be leached from rocks. This chlorine will be nearly free of ^{36}Cl (some ^{36}Cl will be produced naturally by neutron capture), and hence this process will decrease the ^{36}Cl/Cl ratio. Further complications arise from the nuclear bomb-produced ^{36}Cl. Particularly large amounts were produced by nuclear bomb testing at sea, where bomb-produced neutrons were captured by ^{35}Cl in seawater.

In a somewhat different application, Paul *et al*. (1986) used ^{36}Cl to determine the accumulation time of dissolved salt in the Dead Sea. The Dead Sea is a particularly simply hydrologic system because it has no outlet. In such a simple system, we can describe the variation of the number of ^{36}Cl atoms with time as the rate of input less the rate of decay:

$$\frac{dN}{dt} = I - \lambda t \qquad (8.58)$$

where I is the input rate (precipitation of chloride is assumed negligible). Integration of this equation yields:

$$N = \frac{I}{\lambda}(1 - e^{-\lambda t}) \qquad (8.59)$$

Paul *et al*. (1986) measured ^{36}Cl/Cl in Mt. Hermon snow, in various rivers in the Dead Sea system, and in saline springs in the Dead Sea basin. These results are summarized in Table 8.6. Using eqn. 8.58, they estimated an accumulation time of 20,000 years for the salt in the Dead Sea. The Dead Sea basin has been estimated to be 15,000 years old based on ^{14}C. The difference suggests that some of the Cl now in the Dead Sea was inherited from its less saline Pleistocene predecessor, Lake Lisan. The data in Table 8.6 also illustrates how a combination of Cl and ^{36}Cl data can distinguish between addition of Cl from rock leaching and evaporation, both of which are processes that will increase the concentration of Cl. Evaporation should not significantly change the ^{36}Cl/Cl ratio, while addition of Cl derived from rock leaching should decrease this ratio. There is a general southward (downstream) increase in Cl concentration in the Jordan River–Dead Sea system. It is apparent from the data in Table 8.6 that this is due to both addition of rock-derived Cl and evaporation.

8.5.3 ^{10}Be in subduction zone studies

One of the unusual uses of cosmogenic nuclides is the use of ^{10}Be to trace sediment subduction (Tera *et al*., 1986). Since ^{10}Be does not exist in the Earth's interior, its presence there could result only from subduction of sediment (which concentrates cosmogenic

Table 8.6 ^{36}Cl measurements in the Dead Sea system.

Site	^{36}Cl/Cl (10^{-15}) mg/l	Cl 10^6 atoms/l	^{36}Cl
Mt. Hermon Snow	1580 ± 120	1.50	40 ± 5
Banias River	400 ± 60	11.9	80 ± 15
Snir River	430 ± 125	11.0	80 ± 20
Dan River	725 ± 140	10.5	129 ± 25
Lake Kinneret	49 ± 15	252	210 ± 65
Jordan River	121 ± 19	646	1320 ± 210
Dead Sea	17 ± 2	2.30×10^5	6.6×10^4
Ashlag Spring (saline spring)	4 ± 2	2.6×10^5	

Reprinted by permission from McMillan Publishers Ltd: Paul *et al*. (1986).

^{10}Be). ^{10}Be has been identified in some island arc volcanics, but not in other volcanic rocks (at least not above the background level of 10^6 atoms per gram, i.e., 1 atom in 10^{18}). This is strong evidence that subducted sediment plays a role in island arc magma genesis, something suspected on the basis of other geochemical evidence. We will discuss this in more detail in Chapter 11.

8.5.4 Cosmic-ray exposure ages of meteorites

The surfaces of meteorites in space are subject to a fairly high cosmic ray flux because there is no atmosphere to protect them. This leads to another interesting application of cosmogenic isotopes: "cosmic ray exposure ages". Here rare stable isotopes are used rather than radioactive ones because of the long times involved. For example, potassium is not present naturally in iron meteorites, but is produced by cosmic ray interactions. Knowing the production rate of ^{41}K and its abundance, it is possible to calculate how long a meteorite has been exposed to cosmic rays. Two important results of such studies are worth mentioning: (1) exposure ages are much younger than formation ages; and (2) meteorites that are compositionally and petrologically similar tend to have similar exposure ages (Figure 8.26). This means meteorites now colliding with the Earth have not existed as small bodies since the solar system formed. Instead, they are probably more or less continually (on a time-scale of 10^9 yr) produced by breakup of larger bodies through collisions. Also, similar meteorites probably come from the same parent body.

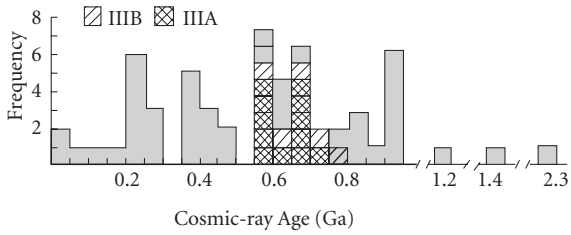

Figure 8.26 Cosmic-ray exposure age distribution in iron meteorites. Seventeen of 18 IIIAB irons fall in a cluster at 650 ± 100 Ma (after Voshage, 1967). Reproduced with permission.

8.5.5 Fossil radionuclides

There is evidence that many short-lived radionuclides were present in the early solar system. They must have been created shortly before the solar system formed, implying a nucleosynthetic process, such as a red giant star or a supernova event shortly before the formation of the Earth (nucleosynthesis, the processes by which the elements are created, is discussed in Chapter 10). Some of these isotopes (e.g., ^{26}Al) may have been sufficiently abundant that they could have been significant heat sources early in solar system history. Evidence of their existence comes from non-uniform distribution of their daughter products. For example, if ^{26}Mg, the daughter of ^{26}Al, were found be more abundant in an Al-rich phase such as plagioclase or spinel than in olivine, one might conclude the excess ^{26}Mg was produced by the decay of ^{26}Al. With a couple of exceptions, evidence of these short-lived radionuclides is restricted to meteorites: they had decayed completely before the Earth formed. These fossil radionuclides nevertheless provide very important constraints on the early history of the solar system and we will consider them in detail in Chapter 10. Here we will briefly discuss four short-lived radionuclides that provide important constraints on the composition and early history of the Earth: ^{129}I, which decays to ^{129}Xe with a half-life of 16 Ma, ^{146}Sm, which decays to ^{142}Nd with a half-life of 68 Ma, ^{182}Hf which decays to ^{182}W with a half-life of 6 Ma, and ^{244}Pu which decays (through fission) to heavy isotopes of Xe, particularly ^{136}Xe, with a half-life of 80 Ma.

It has long been known that ^{129}Xe/^{130}Xe and ^{136}Xe/^{130}Xe ratios in some well gases from volcanic areas in the western US and in MORB are higher than in the atmosphere (e.g., Butler *et al.*, 1963). The most reasonable explanation of this is that Xe in the mantle contains more ^{129}Xe and ^{136}Xe produced by radioactive decay of ^{129}I and ^{244}Pu, respectively, than does the atmosphere. Let's focus just on ^{129}Xe as it provides the tightest constraints on early Earth history. The atmosphere, of course, contains no iodine whereas the mantle does. In this sense, we should not be surprised to find the decay product of ^{129}I in greater amounts in the mantle than the atmosphere. A rule of thumb is that a radionuclide will

decay below detection levels after 5 to 10 half-lives. Thus, essentially all ^{129}I must have been decayed within $16 \times 10 = 160$ Ma of the beginning of the solar system. The atmosphere's deficit in ^{129}X thus suggests that a substantial part of the Xe in the atmosphere has been there since at least 160 Ma after the start of the solar system. That in turn implies the Earth had formed and differentiated and atmosphere had formed by at least that time. Most models of atmospheric evolution explain the Xe isotopic composition of the atmosphere by invoking an "early catastrophic degassing" event very early in Earth's history. While the details of these models differ, all agree that the Earth's atmosphere had formed within the first 100 Ma or so of solar system history (this is not to say that composition of the atmosphere has not evolved since then). An alternative hypothesis proposed that the Earth's atmosphere derives from comet impacts after formation, but that does not explain this difference in Xe isotopic composition.

Small variations in $^{142}Nd/^{144}Nd$ were observed in meteorites, and since these correlated with the Sm/Nd ratio of the material analyzed, it was reasonable to assume these variations were produced by α–decay of ^{146}Sm. The half-life of ^{146}Sm was originally taken to be 103 Ma, but has recently been determined to be 68 ± 7 Ma (Kinoshita *et al.*, 2012). Because of this relatively long half-life of ^{146}Sm, some geochemists thought that $^{142}Nd/^{144}Nd$ variations might also be found in the Earth's oldest rocks. However, only tiny amounts of ^{146}Sm were ever present in the solar system (the solar system initial $^{142}Sm/^{144}Sm$ ratio was only 0.009, and ^{144}Sm is the least abundant stable isotope of Sm!), so very precise measurements were required. In the 1990s, Harvard researchers reported $^{142}Nd/^{144}Nd$ ratios in early Archean rocks from Isua, Greenland, that were higher than the ratio in laboratory standards, but this work could not initially be reproduced in other laboratories. Eventually, however, other workers confirmed anomalously high $^{142}Nd/^{144}Nd$ in Isua rocks. The real surprise, however, came in 2005 when it was demonstrated that all modern mantle-derived rocks and all but a few of the oldest crustal rocks had a uniform $^{142}Nd/^{144}Nd$ ratio that was 20 parts per million higher than in ordinary chondrites (Boyet and Carlson, 2005). Subsequently, O'Neil *et al.* (2008) reported low $^{142}Nd/^{144}Nd$ in meta-igneous rocks of the early Archean Nuvvuagittuq greenstone belt of Labrador. The variations are illustrated in Figure 8.27, where the $^{142}Nd/^{144}Nd$ ratio is expressed in epsilon notation: that it, deviations in parts per 10,000 from a terrestrial standard.

Although non-uniform distribution of ^{142}Nd and ^{146}Sm in the early solar system explains some of the variation in $^{142}Nd/^{144}Nd$ (particularly in different classes of chondritic

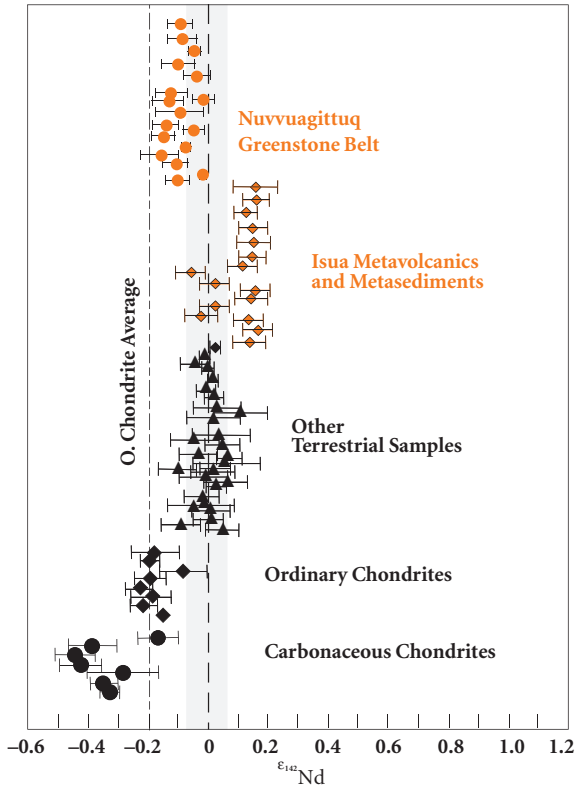

Figure 8.27 Variation of $^{142}Nd/^{144}Nd$ in terrestrial materials and meteorites. All terrestrial rocks younger than about 3.5 billion years have uniform $^{142}Nd/^{144}Nd$ that are about 20 ppm (0.2 parts in 10,000) higher than in ordinary chondrites. Even low ratios are found in early Archean rocks from Isua, Greenland. $^{142}Nd/^{144}Nd$ ratios lower than the modern terrestrial value have been found in the Nuvvuagittuq greenstone belt, Labrador. ε_{142Nd} is the deviation in parts per 10,000 of $^{142}Nd/^{144}Nd$ from a terrestrial laboratory standard.

meteorites), this cannot explain the difference between the Earth and chondrites. The most reasonable interpretation of this result is that the Sm/Nd ratio of the Earth, or at least the part accessible to sampling, is not chondritic, even for refractory lithophile elements such as the rare earths. If the Earth is not chondritic even for these elements, a major cornerstone of estimating the composition of this Earth and in unraveling its history has been overthrown. If only the assessable part of the Earth is not chondritic, it requires that a silicate reservoir of significant size with a low Sm/Nd ratio formed within the first 100 Ma of Earth history and has been completely isolated from the rest of the silicate Earth for the last 4.4 Ga. Boyet and Carlson (2005) suggested that such a reservoir, which they called the Early Enriched Reservoir, formed as a proto-crust early in Earth history, then sank to the bottom of the mantle where it remains. Others, such as O'Neill and Palme (2008), agree that a low Sm/Nd proto-crust formed, but they argue that it was blasted off the Earth's surface by impacts in a process called collisional erosion. We'll discuss this further in Chapter 11.

The final decay scheme we want to mention is the decay of ^{182}Hf to ^{182}W with a half-life of 6 Ma. This is a particularly interesting decay scheme because when planetary bodies differentiate into silicate mantles and iron cores, Hf, a refractory lithophile element, is concentrated in the silicate portions while W, a refractory siderophile element, is concentrated in cores. Iron meteorites, which are pieces of cores of asteroids, typically have low ^{182}W/^{184}W, indicating that these cores formed before ^{182}Hf had entirely decayed. Conversely, achondritic stony meteorites, which are pieces of asteroid mantles, have high ^{182}W/^{184}W because they were depleted in W by core formation that preceded complete decay of ^{182}Hf. In this way, we know that differentiation of protoplanetary bodies into silicate mantles and cores occurred very early in solar system history. Until recently, all analyzed materials from the Earth have had a uniform, high ^{182}W/^{184}W as well, suggesting the Earth's core began to form early (we do not have samples from the Earth's core; if we did, we would expect them to have low ^{182}W/^{184}W). But Touboul *et al*. (2012) have reported ^{182}W/^{184}W ratios in 2.8 billion year old komatiites from Siberia that are 15 ppm higher than the terrestrial value. This suggests that the accretion and core segregation left the Earth's mantle with variable ^{182}W/^{184}W ratios and that some of this heterogeneity survived until at least 2.8 billion years ago. We will explore this in more detail in subsequent chapters.

REFERENCES AND SUGGESTIONS FOR FURTHER READING

Allègre, C.J. and Luck, J.M. 1980. Osmium isotopes as petrogenic and geologic tracers. *Earth and Planetary Science Letters*, 48: 148–54.

Allègre, C.J., Hofmann, A.W. and O'Nions, K. 1996. The argon constraints on mantle structure. *Geophysical Research Letters*, 23: 3555–7.

Allègre, C.J., Sarda, P. and Staudacher, T. 1993. Speculations about the cosmic origin of He and Ne in the interior of the Earth. *Earth and Planetary Science Letters*, 117: 229–33.

Black, S., MacDonald, R. and Kelly, M.R. 1997. Crustal origin for peralkaline rhyolites from Kenya: evidence from U-series disequilibria and Th-isotopes. *Journal of Petrology*, 38: 277–97. doi: 10.1093/petroj/38.2.277.

Bouvier, A., Vervoort, J.D. and Patchett, P.J. 2008. The Lu-Hf and Sm-Nd isotopic composition of CHUR; constraints from unequilibrated chondrites and implications for the bulk composition of terrestrial planets. *Earth and Planetary Science Letters*, 273: 48–57.

Boyet, M. and Carlson, R.W. 2005. ^{142}Nd evidence for early (>4.53 Ga) global differentiation of the silicate Earth. *Science*, 309: 576–81.

Butler, W.A., Jeffery, P.M., Reynolds, J.H. and Wasserburg, G.J. 1963. Isotopic variations in terrestrial xenon. *Journal of Geophysical Research*, 68: 3283–91.

Caro, G. and Bourdon, B. 2010. Non-chondritic Sm/Nd ratio in the terrestrial planets: Consequences for the geochemical evolution of the mantle–crust system. *Geochimica et Cosmochimica Acta*, 74: 3333–49.

Clark, W.B., Beg, M.A. and Craig, H. 1969. Excess ^{3}He in the sea: evidence for terrestrial primordial helium. *Earth and Planetary Science Letters*, 6: 213–30.

Creaser, R.A., Papanastassiou, D.A. and Wasserburg, G.J. 1991. Negative thermal ion mass spectrometry of osmium, rhenium, and iridium. *Geochimica et Cosmochimica Acta*, 55: 397–401.

DePaolo, D.J. 1981. Neodymium isotopes in the Colorado Front Range and crust mantle evolution in the Proterozoic. *Nature*, 291: 193–6.
DePaolo, D.J. and Wasserburg, G.J. 1976. Nd isotopic variations and petrogenetic models. *Geophysical Research Letters*, 3: 249–52.
Dickin, A.P. 1987. Cerium isotope geochemistry of ocean island basalts. *Nature*, 326: 283–4.
Dickin, A. 1995. *Radiogenic Isotope Geochemistry*. Cambridge, Cambridge University Press.
Esser, B.K. and Turekian, K.K. 1993. The osmium isotopic composition of the continental crust. *Geochimica et Cosmochimica Acta*, 57: 3093–104.
Farley, K.A. and Poreda, R.J. 1993. Mantle neon and atmospheric contamination. *Earth and Planetary Science Letters*, 114: 325–39.
Faure, G. 1986. *Principles of Isotope Geology*, 2nd edn. New York, John Wiley & Sons, Ltd.
Gast, P.W. 1960. Limitations on the composition of the upper mantle. *Journal of Geophysical Research*, 65: 1287–97.
Hauri, E.H. and Hart, S.R. 1993. Re-Os isotope systematics of HIMU and EMII oceanic island basalts from the south Pacific Ocean. *Earth and Planetary Science Letters*, 114: 353–71.
Hawkesworth, C.J., Blake, S., Evans, P., *et al*. 2000. Time scales of crystal fractionation in magma chambers – integrating physical, isotopic and geochemical perspectives. *Journal of Petrology*, 41: 991–1006. doi: 10.1093/petrology/41.7.991.
Heiss, J., Condon, D.J., McLean, N. and Noble, S.R. 2012. $^{238}U/^{235}U$ systematics in terrestrial uranium-bearing minerals. *Science*, 335: 1610–14.
Hirt, B., Herr, W. and Hoffmester, W. 1963. Age determinations by the rhenium-osmium method, in *Radioactive Dating*, pp. 35–44. Vienna, International Atomic Energy Agency.
Honda, M., Patterson, D., Doulgeris, A. and Clague, D. 1991. Possible solar noble-gas component in Hawaiian basalts. *Nature*, 349: 149–51.
Huh, C.-A. and Ku, T.-L. 1984. Radiochemical observations on manganese nodules from three sedimentary environments in the north Pacific. *Geochimica et Cosmochimica Acta*, 48: 951–64.
Kinoshita, N., Paul, M., Kashiv, Y., *et al*. 2012. A shorter ^{146}Sm half-life measured and implications for ^{146}Sm-^{142}Nd chronology in the Solar System. *Science*, 335: 1614–17.
Kurz, M.D. 1987. In situ production of terrestrial cosmogenic helium and some applications to gechronology. *Geochimica et Cosmochimica Acta*, 50: 2855–62.
Kurz, M.D., Jenkins, W.J. and Hart, S.R. 1982. Helium isotopic systematics of oceanic islands and mantle heterogeneity. *Nature*, 297: 43–7.
Luck, J.-M., Birck, J.-L. and Allegre, C.J. 1980. ^{187}Re-^{187}Os systematics in meteorites: Early chronology of the solar system and age of the Galaxy. *Nature*, 283: 256–9.
Lupton, J.E. 1983. Terrestrial inert gases: isotopic tracer studies and clues to primordial components in the mantle. *Annual Review of Earth and Planetary Science*, 11: 371–414.
Lupton, J.E. and Craig, H. 1981. A major ^{3}He source on the East Pacific Rise. *Science*, 214: 13–18.
Lupton, J.G. and Craig, H. 1975. Excess ^{3}He in oceanic basalts: evidence for terrestrial primordial helium. *Earth and Planetary Science Letters*, 26: 133–9.
Marshall, B.D. and DePaolo, D.J. 1987. Initial Ca isotope variations in igneous rocks: implications for petrogenetic models and the composition of the lower crust. *EOS*, 68: 465.
Martin, C.E. 1991. Osmium isotopic characteristics of mantle-derived rocks. *Geochimica et Cosmochimica Acta*, 55: 1421–34.
Mattinson, J.M. 2010. Analysis of the relative decay constants of ^{235}U and ^{238}U by multi-step CA-TIMS measurements of closed-system natural zircon samples. *Chemical Geology*, 275: 186–98.
McArthur, J.M., Howarth, R.J. and Bailey, T.R. 2001. Strontium isotope stratigraphy: LOWESS Version 3: best fit to the marine Sr isotope curve for 509 Ma and accompanying look-up table for deriving numerical age. *Journal of Geology*, 109: 155–70.
Nyquist, L.E., Bogard, D.D., Wiesmann, H., *et al*. 1990. Age of a eucrite clase from the Bholghati howardite. *Geochimica et Cosmochimica Acta*, 54: 2195–206.
O'Neil, J., Carlson, R.L., Francis, D. and Stevenson, R.K. 2008. Neodymium-142 evidence for Hadean mafic crust. *Science*, 321: 1828–31.
O'Neill, H.S.C. and Palme, H. 2008. Collisional erosion and the non-chondritic composition of the terrestrial planets. *Philosophical Transactions of the Royal Society A*, 366: 4205–38. doi: 10.1098/rsta.2008.0111, 2008.
Ozima, M. and Zahnle, K. 1993. Mantle degassing and atmospheric evolution: noble gas view. *Geochemical Journal*, 27: 185–200.
Patchett, P.J. 1983. Importance of the Lu-Hf isotopic system in studies of planetary chronology and chemical evolution. *Geochimica et Cosmochimica Acta*, 47: 81–91.

Patchett, P.J., White, W.M., Feldmann, H., Kielinczuk, S. and Hofmann, A.W. 1984. Hafnium/rare earth element fractionation in the sedimentary system and crustal recycling into the Earth's mantle. *Earth and Planetary Science Letters*, 69: 365–78.

Paul, M., Kaufman, A., Magaritz, M., *et al*. 1986. A new ^{36}Cl hydrological model and ^{36}Cl systematics in the Jordan River/Dead Sea system. *Nature*, 321: 511–15.

Peucker-Ehrenbrink, B., Ravissa, G. and Hoffmann, A.W. 1995. The marine ^{187}Os/^{186}Os record of the past 80 million years. *Earth and Planetary Science Letters*, 130: 155–67.

Poreda, R.J. and Farley, K.A. 1992. Rare gases in Samoan xenoliths. *Earth and Planetary Science Letters*, 113: 129–44.

Reisberg, L., Zindler, A., Marcantonio, F., *et al*. 1993. Os isotope systematics in ocean island basalts. *Earth and Planetary Science Letters*, 120: 149–67.

Renne, P.R., Mundil, R., Balco, G., Min, K. and Ludwig, K.R. 2010. Joint determination of ^{40}K decay constants and ^{40}Ar*/^{40}K for the Fish Canyon sanidine standard, and improved accuracy for ^{40}Ar/^{39}Ar geochronology. *Geochimica et Cosmochimica Acta*, 74: 5349–67. doi: 10.1016/j.gca.2010.06.017.

Sarda, P., Staudacher, T. and Allègre, C.J. 1988. Neon isotopes in submarine basalts. *Earth and Planetary Science Letters*, 91: 73–88.

Tera, F., Brown, L., Morris, J., *et al*. 1986. Sediment incorporation in island-arc magmas: inferences from ^{10}Be. *Geochimica et Cosmochimica Acta*, 50: 535–50.

Touboul, M., Puchtel, I.S. and Walker, R.J. 2012. ^{182}W evidence for long-term preservation of early mantle differentiation products. *Science*, 335: 1065–9.

Vervoort, J.D. and Blichert-Toft, J. 1999. Evolution of the depleted mantle; Hf isotope evidence from juvenile rocks through time. *Geochimica et Cosmochimica Acta*, 63: 533–56.

Voshage, H. 1967. Bestrahlungsalter und Herkunft der Eisenmeteorite. *Zeitschrift. Naturforschung*, 22a: 477–506.

Walker, R.J., Carlson, R.W., Shirey, S.B. and Boyd, F.R. 1989. Os, Sr, Nd, and Pb isotope systematics of southern African peridotite xenoliths: implications for the chemical evolution of the subcontinental mantle. *Geochimica et Cosmochimica Acta*, 53: 1583–95.

Walker, R.J., Morgan, J.W., Naldrett, A.J., Li, C. and Fassett, J.D. 1991. Re–Os isotope systematics of Ni–Cu sulfide ores, Sudbury igneous complex: evidence for a major crustal component. *Earth and Planetary Science Letters*, 105: 416–29.

White, W.M., Patchett, P.J. and BenOthman, D. 1986. Hf isotope ratios of marine sediments and Mn nodules: evidence for a mantle source of Hf in seawater. *Earth and Planetary Science Letters*, 79: 46–54.

York, D. 1969. Least squares fitting of a straight line with correlated errors. *Earth and Planetary Science Letters*, 5: 320–24.

Zindler, A. and Hart, S.R. 1986. Helium: problematic primordial signals. *Earth and Planetary Science Letters*, 79: 1–8.

PROBLEMS

1. A few years ago, chemists at the University of Utah claimed to have succeeded with a "cold" fusion experiment in which deuterium nuclei fuse to produce a ^{3}He nucleus and a neutron, i.e.:

$$^{2}\mathrm{H} + {}^{2}\mathrm{H} \rightarrow {}^{3}\mathrm{He} + \mathrm{n}$$

If the mass of ^{2}H is 2.0141077 u, the mass of ^{3}He is 3.01602929 u, the mass of a neutron is 1.00866489 u, and normal water has $^{2}\mathrm{H}/^{1}\mathrm{H} = 1.4 \times 10^{-4}$, what is the energy yield (in kJ) of this reaction per mole of normal water? (Don't forget that each reaction requires two deuterons.)

2. What are the binding energies per nucleon of ^{147}Sm (mass = 146.914907 u) and ^{143}Nd (mass = 142.909823 u)?

3. Calculate the maximum β^- energy in the decay of ^{87}Rb to ^{87}Sr. The mass of ^{87}Rb is 86.9091836 u; the mass of ^{87}Sr is 86.9088902 u.

4. What is the decay constant (λ) of ^{152}Gd if its half-life is 1.1×10^{14} yr?

5. The following data were measured on whole rock gneiss samples from the Bighorn Mountains of Wyoming. Use linear regression to calculate the age and initial $^{87}Sr/^{86}Sr$ for this gneiss.

Sample	$^{87}Rb/^{86}Sr$	$^{87}Sr/^{86}Sr$
4173	0.1475	0.7073
3400	0.2231	0.7106
7112	0.8096	0.7344
3432	1.1084	0.7456
3422	1.4995	0.7607
83	1.8825	0.7793

6. The following were measured on a komatiite flow in Canada. Use simple linear regression to calculate slope. Plot the data on isochron diagrams.

	$^{147}Sm/^{144}Nd$	$^{143}Nd/^{144}Nd$
M654	0.2427	0.513586
M656	0.2402	0.513548
M663	0.2567	0.513853
M657	0.2381	0.513511
AX14	0.2250	0.513280
AX25	0.2189	0.513174
M666	0.2563	0.513842
M668	0.2380	0.513522

   (**a**) Calculate the Sm–Nd age and the error on the age.
   (**b**) Calculate the initial ε_{Nd} (i.e., the ε_{Nd} at the age calculated above) and the error on the initial ε_{Nd}.

7. A sample of granite has $^{143}Nd/^{144}Nd$ and $^{147}Sm/^{144}Nd$ of 0.51215 and 0.1342, respectively. The present chondritic $^{143}Nd/^{144}Nd$ and $^{147}Sm/^{144}Nd$ are 0.512638 and 0.1966, respectively. The decay constant of ^{147}Sm is $6.54 \times 10^{-12}\,yr^{-1}$. Calculate τ_{CHUR} (i.e., the crustal residence time relative to a chondritic mantle) for this granite.

8. Imagine that an initially uniform silicate Earth underwent melting at some time in the past to form continental crust (melt) and mantle (melting residue). Calculate the present-day Sr and Nd isotopic composition of 1%, 2%, and 5% partial melts and respective melting residues, assuming the bulk partition coefficients given in Example 8.4. Assume that the present-day $^{87}Rb/^{86}Sr$, $^{87}Sr/^{86}Sr$, $^{147}Sm/^{144}Nd$, $^{143}Nd/^{144}Nd$ ratios of the bulk silicate Earth are 0.076, 0.704, 0.202, and 0.51282 respectively. Perform the calculation assuming the melting occurred at 4.0 Ga, 3.0 Ga, and 2.0 Ga. Plot your results on a Sr–Nd isotope diagram (i.e., $^{143}Nd/^{144}Nd$ vs. $^{87}Sr/^{86}Sr$).

9. Given the data on a series of whole rocks below, use linear regression to calculate:

   (**a**) the age of the rocks and the error on the age;
   (**b**) their initial $^{143}Nd/^{144}Nd$, and the error on the initial ratio.
   (**c**) From (b), calculate the initial ε_{Nd}, that is, ε_{Nd} at the time calculated in (a). Take the present-day chondritic $^{143}Nd/^{144}Nd$ to be 0.512638 and the (present-day) chondritic $^{147}Sm/^{144}Nd$ to be 0.1967 (you need to calculate the chondritic value at the time the rock formed to calculate initial ε_{Nd}).

(**d**) Calculate the depleted mantle model age τ_{DM}. Assume that the present $^{143}Nd/^{144}Nd$ of the depleted mantle is 0.51310, and that the depleted mantle has evolved from the chondritic initial with a constant $^{147}Sm/^{144}Nd$ since 4.55 Ga. How does it compare with the age you calculated in (a)?

Sample	$^{147}Sm/^{144}Nd$	$^{143}Nd/^{144}Nd$
Whole rock	0.1886	0.512360
Garnet	0.6419	0.513401
Clinopyroxene	0.1146	0.512245

Linear regression functions are available on some scientific calculators and in statistical packages for personal computers, and in Microsoft Excel.

10. The following were measured on a komatiite flow in Canada. Use simple linear regression to calculate slopes. Plot the data on isochron diagrams.

	$^{206}Pb/^{204}Pb$	$^{207}Pb/^{204}Pb$	$^{208}Pb/^{204}Pb$
M665	15.718	14.920	35.504
M654	15.970	14.976	35.920
M656	22.563	16.213	41.225
M663	16.329	15.132	35.569
M657	29.995	17.565	48.690
AX14	32.477	17.730	49.996
AX25	15.869	14.963	35.465
M667	14.219	14.717	33.786
M666	16.770	15.110	35.848
M668	16.351	15.047	36.060
M658	20.122	15.700	39.390

(**a**) Calculate the Pb–Pb age and the error on the age.
(**b**) Calculate the Th/U ratio of the samples.

11. Calculate the $^{207}Pb/^{204}Pb$–$^{206}Pb/^{204}Pb$ age for the rocks below. (*Hint*: first calculate the slope using linear regression, then use Excel's Solver to calculate the age.)

Sample	$^{206}Pb/^{204}Pb$	$^{207}Pb/^{204}Pb$
NPA5	15.968	14.823
NPA12	17.110	15.043
NPA15	17.334	15.085
NPA15HF	17.455	15.107

12. (**a**) Calculate the isotopic evolution ($^{207}Pb/^{204}Pb$ and $^{206}Pb/^{204}Pb$ only) of Pb in a reservoir having a $^{238}U/^{204}Pb$ of 8. Do the calculation at 0.5 Ga intervals from 4.5 Ga to present. Assume the reservoir started with Canyon Diablo initial Pb isotopic composition. Plot your results on a $^{207}Pb/^{204}Pb$ vs. $^{206}Pb/^{204}Pb$ graph.
(**b**) Calculate the isotopic evolution ($^{207}Pb/^{204}Pb$ and $^{206}Pb/^{204}Pb$ only) of Pb in a reservoir having a $^{238}U/^{204}Pb$ of 7 from 4.5 to 2.5 Ga and $^{238}U/^{204}Pb$ of 9 from 2.5 Ga to present. Do the calculation at 0.5 Ga intervals from 4.5 Ga to present. Assume the reservoir started with Canyon Diablo initial Pb isotopic composition. Plot your results on a $^{207}Pb/^{204}Pb$ vs. $^{206}Pb/^{204}Pb$ graph.

HINT: The equation

$$^{206}\mathrm{Pb} / {}^{204}\mathrm{Pb} = {}^{206}\mathrm{Pb} / {}^{204}\mathrm{Pb}_0 + \mu(e^{\lambda_{238}t} - 1)$$

is valid for calculating the growth of $^{206}Pb/^{204}Pb$ only between the present and the initial time; i.e., the time when $^{206}Pb/^{204}Pb = (^{206}Pb/^{204}Pb)_o$ (because the $^{238}U/^{204}Pb$ ratio used is the present ratio). The growth of $^{206}Pb/^{204}Pb$ between two other times, t_1 and t_2, where t_1 is older than t_2, may be calculated by taking the growth of $^{206}Pb/^{204}Pb$ between t_2 and the present, and between t_1 and the present, and subtracting the latter from the former. If μ_1 is the value of μ between t_1 and t_2, and μ_2 is the value of μ between t_2 and the present, the relevant equation is then:

$$^{206}\mathrm{Pb} / {}^{204}\mathrm{Pb} = (^{206}\mathrm{Pb} / {}^{204}\mathrm{Pb})_{t_1} + \mu_1(e^{\lambda_{238}t_1} - 1) + \mu_2(e^{\lambda_{238}t_2} - 1)$$

if $\mu_1 = \mu_2$ then the equation simplifies to:

$$^{206}\mathrm{Pb} / {}^{204}\mathrm{Pb} = (^{206}\mathrm{Pb} / {}^{204}\mathrm{Pb})_{t_1} + \mu(e^{\lambda_{238}t_1} - e^{\lambda_{238}t_2})$$

13. Show that when $\lambda_D >> \lambda_P$ and $t << 1/\lambda_P$, eqn. 8.37 reduces to eqn. 8.52 (with D referring to daughter ^{230}Th, and P referring to parent ^{238}U).

14. A basalt from Réunion has a (^{230}Th/^{232}Th) ratio of 0.93 and a (^{238}U/^{232}Th) ratio of 0.75. Assuming the age of the basalt is 0:

(**a**) What is the (^{238}U/^{232}Th) ratio of the source of the basalt?
(**b**) What is the ^{232}Th/^{238}U *atomic* ratio of the source of the basalt?
(**c**) Assuming bulk distribution coefficients of 0.01 for U and 0.005 for Th and equilibrium melting, what is the percent melting involved in generating this basalt?
(remember the parentheses denote *activity* ratios).

15. Given the following data on the Cheire de Mazaye Flow in the Massif Central, France, calculate the age of the flow and the initial ^{232}Th/^{238}U (atomic). Use simple linear regression in obtaining your solution.

	(^{238}U/^{232}Th)	(^{230}Th/^{232}Th)
Whole rock	0.744	0.780 ± 0.012
Magnetite M1 (80-23μ)	0.970	0.864 ± 0.017
Magnetite M2 (23-7μ)	1.142	0.904 ± 0.017
Clinopyroxene	0.750	0.791 ± 0.019
Plagioclase	0.685	0.783 ± 0.018